Comparative Methods for Quantifying Myocardial Infarct Size by Thallium-201 SPECT

Florence Prigent, Jamshid Maddahi, Ernest V. Garcia,* Kenneth Resser, Allan S. Lew, and Daniel S. Berman

Department of Medicine, Division of Cardiology, and the Department of Nuclear Medicine, Cedars-Sinai Medical Center, and the Department of Medicine, University of California, School of Medicine, Los Angeles, California

Maximum-count circumferential profile analysis of ^{201}Tl single photon emission computed tomograms (SPECT) was employed to quantify infarct size (*15*) in ten dogs with acute closed chest coronary occlusion (seven left anterior descending coronary artery and three left circumflex coronary artery) who underwent rest-redistribution ^{201}Tl SPECT. The extent of hypoperfused myocardium was calculated as a percentage of slice mass on rest-redistribution ^{201}Tl SPECT. Pathologic IS was determined by triphenyl tetrazolium chloride (TTC) staining. On each tomogram, SPECT IS was defined as the % of the maximum-count circumferential profile points falling below normal. To calculate total LV infarct size, slice ISs were added to one another after each was multiplied by a coefficient K that reflected the contribution of that slice to the total left ventricular mass. K was derived from an observed relationship in normal dogs between slice fractional distance from the apex and either (a) its actual weight, (b) its geometric SPECT area, or (c) its count-based SPECT area, the assessment of which was independent of edge detection. Using any of these algorithms, there was a high linear correlation between the tomographic and TTC IS. A similar algorithm was also developed from tomograms of eight normal patients. These data offer promise for the clinical noninvasive assessment of the extent of hypoperfused myocardium.

J Nucl Med 28:325–333, 1987

Noninvasive assessment of the extent of myocardial infarction may guide therapeutic interventions and provide prognosis information (*1–5*). Several nonimaging (*6–9*) and imaging (*8–20*) techniques have been applied for measurement of infarct size. Using thallium-201 single photon computed rotational tomographic (^{201}Tl SPECT) technique, we have previously applied maximum-count circumferential profile analysis for the quantification of the extent of experimental myocardial infarction on individual tomographic slices (*21*). In this study, we (a) developed tomographic image-based algorithms for determination of the contribution of myocardial slices to the total left ventricular mass in normal canine hearts, (b) applied these algorithms for the assessment of experimental left ventricular infarct size, and (c) determined whether or not similar image-based algorithm could be developed from the tomographic data of normal human subjects.

MATERIALS AND METHODS

Experimental Protocol

Sixteen dogs (16 to 32 kg) were studied, six controls and ten with acute myocardial infarction. Anesthesia was induced and maintained with i.v. administration of sodium pentobarbital (25 mg/kg for induction). Myocardial infarction was produced by closed-chest occlusion of a coronary vessel as follows. Femoral arterial pressure and peripheral-lead electrocardiogram were monitored continuously. Heparin (100 IU/kg) was administered hourly. A modified 7F Judkins' angiographic catheter was introduced into the left common carotid artery and advanced under fluoroscopic control into the ostium of the left anterior descending coronary artery (LAD) in seven dogs or the left circumflex artery (LCX) in three dogs.

Received Aug. 27, 1985; revision accepted Sept. 4, 1986.

For reprints contact: Jamshid Maddahi, MD, Cardiology-Nuclear Medicine, Cedars-Sinai Med. Ctr., 8700 Beverly Blvd., Los Angeles, CA 90048.

*Present address: Emory University, Atlanta, GA.

An inflatable balloon-tipped 2F Fogarty catheter was then passed through the angiographic catheter and positioned into the coronary artery to occlude the vessel at different levels from the ostium. The occlusion was maintained for at least 6 hr before thallium imaging and was continued until dogs were killed.

Imaging Protocol

The dogs were put on the imaging table in the right anterior oblique position. Two millicuries of ^{201}Tl were injected intravenously and tomography was performed in vivo 10 min after injection. A large field-of-view camera† was used equipped with 75 photomultiplier tubes, a ¼-in.-thick NaI (Tl) crystal, and an all-purpose, parallel-hole collimator. Two 20% energy windows positioned on the 68–80 keV and 160 keV photopeaks were used. The collimator was rotated 180° around the dog's chest from the left lateral to the right lateral position to obtain 30 projections spaced by 6° each. Each projection was acquired for 30 sec. The data were stored in a 64 × 64 × 16 bit matrix. The extrinsic full width half maximum (FWHM) measured with a line source at 8 in. was 18 mm in air for ^{201}Tl. The pixel size was 0.434 × 0.434 cm.

Postmorten Infarct Size Assessment

Immediately after imaging, the dogs were killed by i.v. injection of potassium chloride and the hearts were excised and cut into 6 to 12 mm thick slices perpendicular to the long axis of the left ventricle. The slices were incubated for 10 min in triphenyl tetrazolium chloride (TTC). We used TTC for pathological infarct size assessment since several studies have demonstrated the validity of TTC staining for determination of myocardial infarct size in dogs, 6–8 hr after coronary occlusion (*22,23*). The size of the TTC-defined infarct was measured by planimetry in each myocardial slice on its basal side by an experienced technologist unaware of the scintigraphic findings. To express the TTC slice infarct size in grams, the % infarcted area of the basal and apical side (the latter being measured on the basal side of the preceding slice) were averaged and the resulting % infarcted area was multiplied by the slice mass. To obtain the % TTC infarct size for the entire myocardium, the infarct mass of all slices were added together and the total infarct mass was divided by the total left ventricular mass.

Tomographic Cut Infarct Size Assessment

The infarct size in individual tomograms was assessed according to our previously described technique (*21*). Briefly, each of the 30 projections was corrected for nonuniformity with a 30 million-count image of a cobalt-57 source and adjusted for center of rotation. Projections were filtered back-projected using a low-resolution Hanning filter to obtain transaxial tomograms. Then the transaxial tomograms were nine-point smoothed (4-2-1 weighing) and then reoriented into vertical long-axis and short-axis tomograms, parallel and perpendicular to the long-axis of the left ventricle (*24*). Myocardial activity was analyzed from the short axis profiles, except for the apex, which was analyzed from the apical portion of the vertical long-axis profiles. Maximum-counts circumferential profiles were extracted from the tomograms and compared to previously established normal limits. The infarct size (in %) was defined by the % of circumferential profile points falling below a threshold that had demonstrated a high correlation ($r = 0.95$, $p < 0.001$) between the pathologic and tomographic infarct size in 15 calibration slices of infarcted dogs in a previous study (*21*).

Total Left Ventricular Infarct Size Assessment

To assess left ventricular infarct size, the infarct size on each slice had to be summed. Since the circumferential profiles analysis technique results in the infarct size given as a percentage, the difference in myocardial slice mass from apex to base has to be taken into consideration. As shown on Figure 1, when the left ventricle is sliced at equidistant intervals, perpendicular to the long axis of the heart, slice mass differs from apex to base because of varying slice radius and myocardial wall thickness. Thus, it was postulated that each myocardial slice would represent a certain fraction of the left ventricular mass according to its fractional distance along the long-axis of the left ventricle. Therefore, the number of abnormal profile points on each tomogram (Ap_{apex}, Ap_1, Ap_2, $\cdots$) was multiplied by a coefficient K, reflecting the contribution of each myocardial slice to the total left ventricular mass and then summed. K for a particular slice was defined by the ratio of the slice mass over the heaviest slice mass. This sum was divided by the total number of left ventricular profile points corrected for K according to the formula:

$$\% \text{ IS} = \frac{Ap_{apex}(K_{apex}) + Ap_1(K_1) + Ap_2(K_2) + \cdots}{Tp_{apex}(K_{apex}) + 60\,(K_1 + K_2 + K_3 \cdots)},$$

where Ap = number of abnormal points in the apex (Ap_{apex}) and short-axis cuts numbered from the most apical to the most basal (Ap_1, $Ap_2 \cdots$), K = correction factor for the apex (K_{apex}) and short-axis cuts (K_1, $K_2 \cdots$). Tp_{apex} = total number

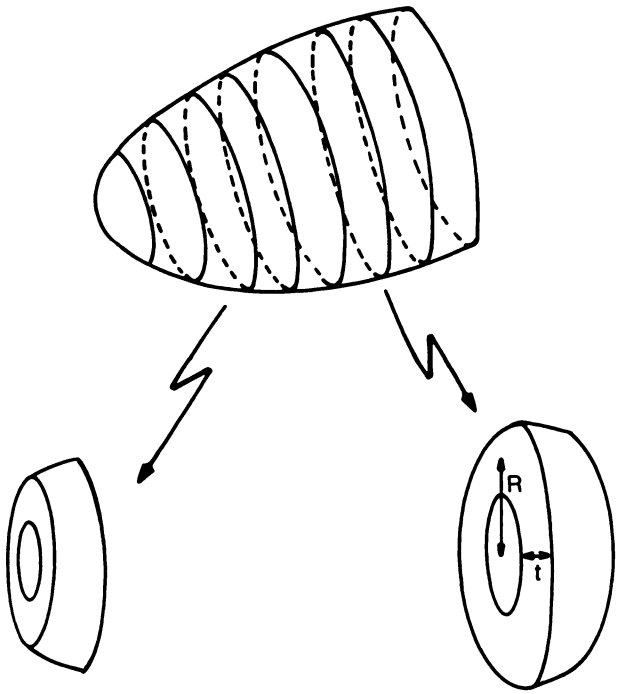

FIGURE 1
Varying myocardial slice mass from apex to base. For similar slice thickness, each slice mass is dependent on the mean radius and myocardial wall thickness.

of points in the apex, 60 = number of points per short-axis slice, K_1, K_2 = K factor for short-axis slice 1, 2 ···.

In order to determine K, three algorithms expressing the difference in mass of equal thickness myocardial slices from apex to base were developed. Algorithm 1 related the % slice mass to its distance from the left ventricular apex; Algorithms 2 and 3 related the % slice surface area to its distance from the left ventricular apex. Subsequently, Algorithms 1 through 3 were used to calculate total left ventricular infarct size (respectively, methods 1 through 3).

Algorithm 1

This algorithm, described in a previous study (*25*), will be the reference algorithm here. It was developed from the post-mortem data of the five control dogs in which data was available for measurement. To express the contribution of each myocardial slice to the total left ventricular mass, the actual mass of each myocardial slice was expressed as a percent of the heaviest slice in a given heart and plotted as a function of the fractional distance of the slice along the left ventricular long axis. Polynomial regression analysis was applied to define the relationship between the % mass (K) and the fractional distance for each dog and for all dogs pooled.

Algorithm 2

This algorithm was developed from the tomographic data of the six control dogs to reflect the relative slice mass from its scintigraphic geometric slice area. The rationale was the following. Since slice mass is proportional to slice volume, the slice volume should vary with slice distance similarly as slice mass varies with slice depth. In addition, if all slices have the same thickness along the left ventricular long-axis, which is the case for the tomograms (that are all 1 pixel thick), slice area and slice volume are proportional and slice area should vary with distance in a fashion similar to slice mass. Thus, slice area was calculated on the short-axis tomograms as $S = \pi \cdot d \cdot t$ (see Appendix) where d = slice mean diameter and t = myocardial wall thickness (along the short axis of the slice) (Fig. 2). The distance (in pixels) between the two peak activities on the count profile across the center of the slice was defined as "d". To measure myocardial wall thickness, the operator drew manually two vertical profiles on the epicardial and endocardial edges of the two opposite walls adjacent to the interventricular septum and t was given by the average distance in pixels between the two profiles. At the level of the apex where no ventricular cavity was present, S was measured as $S = \pi(d^1/2)^2$, where d^1 = entire diameter of the slice.

The most basal slice was defined as that beyond which the pattern of ^{201}Tl uptake became crescent-shaped (less than half-circle) or became fragmented.

Subsequently, the slice surface expressed as a % of the largest slice was plotted as a function of slice fractional distance from the apex. Polynomial regression analysis was applied to the relationship % slice area versus fractional distance in each dog and for all dogs pooled together. In this method, the measurement of wall thickness was dependent on edge detection.

Algorithm 3

The aim of this approach was to develop an algorithm independent of edge detection. This algorithm reflected the relative slice mass from its tomographic area approximated by a count-based technique: It has been previously shown that

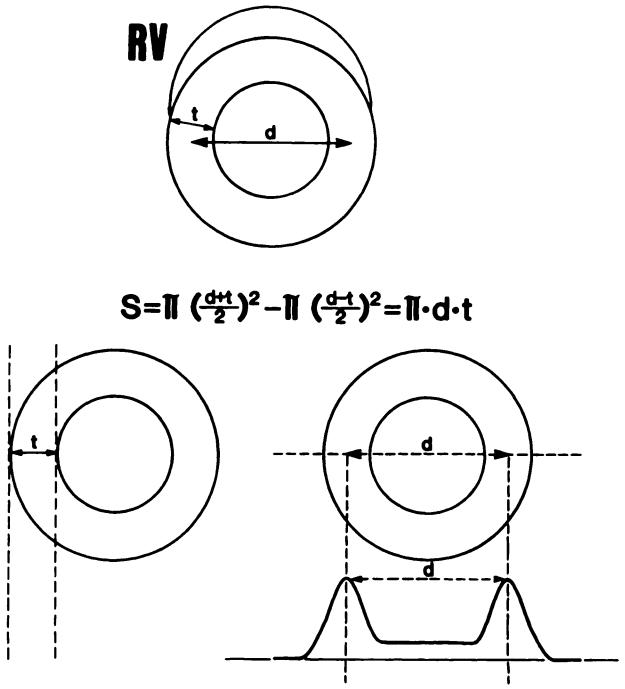

FIGURE 2
Determination of myocardial slice surface area on a short-axis tomogram. The slice surface area is calculated as $S = \pi \cdot d \cdot t$, with d = mean diameter and t = myocardial wall thickness. d is defined by the distance in pixel between the two peak activities on a profile drawn through the center of the slice. t is measured by drawing two vertical profiles on the endocardial and epicardial side of the two walls adjacent to the interventricular septum (RV = right ventricle) and averaging the two measurements. Of note, in dogs, the right ventricle is located above the left ventricle, thus the interventricular septum is the upper wall.

in positron emission tomography (PET) imaging, the counts recovered from the tomograms are dependent on object size (*26,27*), for object smaller than twice the FWHM, when using high-, medium-, or low-resolution filters. Similar near-linear dependence was found in SPECT imaging (*28*) with the recovered counts from technetium-99m- (^{99m}Tc) filled spheres or ^{99m}Tc wedge-phantom imaged by a device similar to the one used in the present study. In our experiment, myocardial wall thickness or myocardial slice thickness never exceeded 30 mm; thus it was always <2 FWHM (36 mm). Thus we postulated that the dependence of the recovered counts on object size should also exist with ^{201}Tl SPECT and that the maximum count vale (C) found in each normal tomogram, would reflect the myocardial wall thickness (t). Therefore, the formula S = ii.t.d from Algorithm 2 was modified by substituting C (maximum count value) for t to yield a "count-based slice area" defined as S = ii.C.d. Subsequently, the count-based slice area, normalized to the greatest slice area for a given heart, was plotted as a function of fractional slice distance from the apex. Polynomial regression analysis was applied to the data in a similar fashion as in Algorithms 1 and 2.

Clinical Protocol

In eight patients with a <1% calculated likelihood of coronary artery disease (*29,30*), 2 mCi of ^{201}Tl were injected

intravenously at the peak of a symptom-limited exercise and exercise continued 1 min after injection. Imaging was started 10 min after the end of exercise. Imaging and reconstruction protocols were similar to those of the experimental protocol. On the reconstructed tomograms, slice mean diameter and maximum counts were measured and count-based slice area was then calculated. The dependence of count-based slice area on fractional slice distance from the apex was assessed in a similar fashion as in Algorithm 3 of the experimental protocol.

Statistical Analysis

Statistical analysis was carried out using BMDP and SAS statistical software packages (*31,32*).

1. Polynomial regression analysis was applied to define a functional relationship between myocardial slice mass and its distance from the apex (Algorithm 1) and to determine the polynomial degree which best fit the data. In a similar fashion, the analysis was applied to define the dependence of, respectively, myocardial slice geometric area and slice distance from the apex (Algorithm 2) and count-based slice area on its distance from the apex (Algorithm 3). The comparison of individual dog polynomial regressions was carried out using analysis of variance (*31*) of regression coefficients over the different dogs.

2. The pathologic and tomographic infarct sizes for each of the three methods were compared using least squares linear regression analysis and by simultaneously testing if the slope differed from 1 and if the y-intercept differed from 0 (multivariate F test) (*32,33*) for the regression of tomography on pathologic infarct size. The s.e.e. measured the random variability in tomographic infarct size given the pathologic infarct size (*33*). The relative bias represented the mean difference between the pathologic and tomographic infarct size for a given method. The relative precision for a given method represented the s.d. of the relative bias (i.e., the s.d. of the difference). All p values were two-tailed.

RESULTS

Pathology

Table 1 summarizes the pathologic results for all 16 dogs. The mean heart mass was 82 ± 9 g (mean ± s.d.) for the control dogs and 93 ± 27 g for the infarcted dogs. The infarct mass ranged from 8 to 40 g, representing 9% to 31% of the left ventricle. The mean infarct mass was 23 ± 9 g in dogs with LAD necrosis and 17 ± 7 g for the dogs with LCX occlusion.

Algorithm 1

In the control dogs a consistent relationship was observed between fractional slice distance and slice weight so that the mass of each slice increased with increasing fractional distance from the apex to the mid-ventricular region and then decreased (Fig. 3). A second-degree equation fit the data best or was no worse than a higher degree equation for the five dogs. The five equations did not differ significantly from each other, so a pooled second degree polynomial equation was fit to all of the data as K (in %, for a particular slice) = $-0.023X^2 + 2.94X - 1.2$ ($r^2 = 0.87$, s.e.e. = 10%) where X is the fractional slice distance from the apex. This equation was referred to as Eq. 1. We concluded that K for a given slice could be predicted from its fractional distance along the left ventricular long axis.

TABLE 1
Pathologic Measurements in 16 Dogs

Dog no.	Heart weight (g)	Infarct weight (g)	Infarct size (%)
Control			
1	—	0	0
2	79	0	0
3	68	0	0
4	86	0	0
5	95	0	0
6	84	0	0
LAD occlusions			
7	109	28	26
8	165	40	24
9	84	27	31
10	82	10	13
11	91	24	26
11	91	24	26
12	71	14	20
13	64	19	30
LCX occlusions			
14	83	24	29
15	97	19	19
16	87	8	9

Algorithm 2

A consistent relationship was observed between the geometric slice surface area and fractional distance from

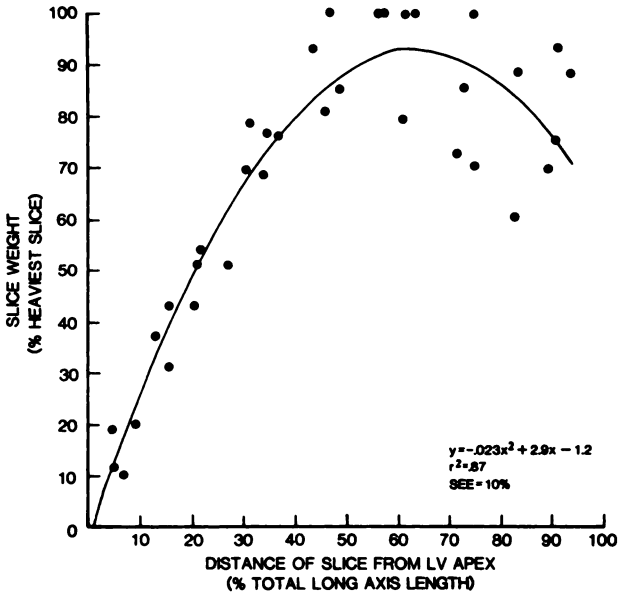

FIGURE 3
Dependence of myocardial slice mass on its distance from the left ventricular apex in the five control dogs. A second-degree equation best described this relationship.

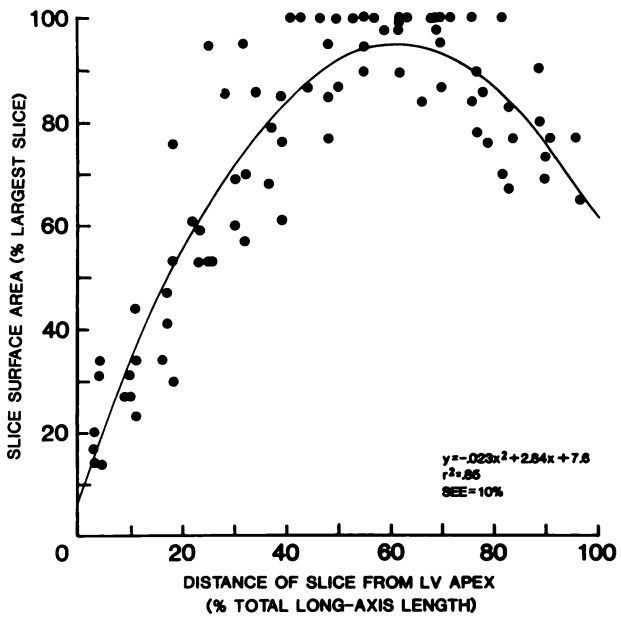

FIGURE 4
Dependence of myocardial slice geometric surface area on its distance from the left ventricular apex in the six control dogs. A second degree equation best described the data.

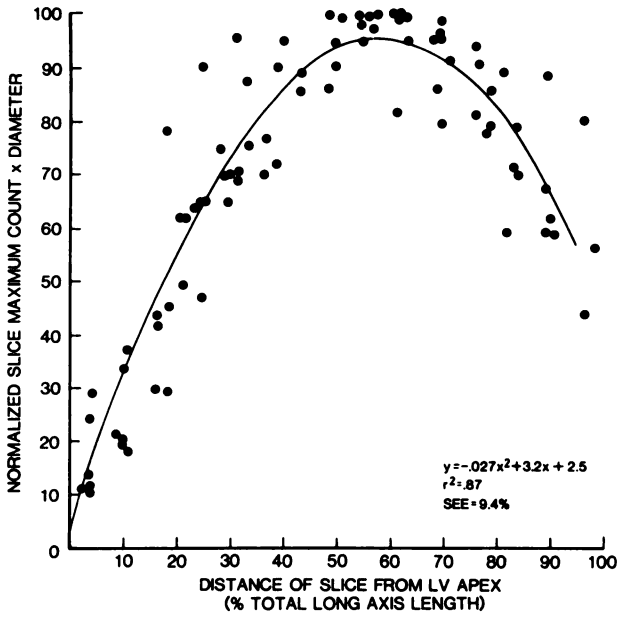

FIGURE 5
Dependence of myocardial slice count-based surface area on its distance from the left ventricular apex in the six control dogs. A second degree equation best described the data.

the apex in the six control dogs. Slice area initially increased with distance from the apex to the mid-ventricular region and then decreased (Fig. 4). For five of six dogs the best fit was a second degree equation. For each individual dog, the equations weight versus fractional distance and area versus fractional distance did not differ significantly except for one dog. When the individual equations were pooled, a second degree equation: K (in %) = $-.023X^2 + 2.8X + 7.6$ ($r^2 = 0.85$, s.e.e. = 10%) best described the data [Eq. (2)]. This pooled equation was not significantly different from Eq. (1) ($p = 0.4$). Thus, we concluded that the relative geometric slice area reflected the relative mass of a myocardial slice and allowed the determination of K.

Algorithm 3

A consistent relationship was observed between count-based slice area and its fractional distance from the apex in the six control dogs. Count-based slice area initially increased with distance to the mid ventricular region and then decreased at proximity of the base (Fig. 5). For five of six dogs, the best fit was also a second degree equation. The individual equations for % count-based versus fractional distance did not differ significantly from the equations % geometric area versus fractional distance in five of six dogs (Algorithm 2) and from the equations % weight versus fractional distance in four of the five dogs for which the pathologic data was available (Algorithm 1). When all the equations were pooled, a second degree equation fit the data best as K = $-0.027X^2 + 3.2X + 2.5$ ($r^2 = 0.87$, s.e.e. = 9.4%) [Eq. (3)]. The pooled equation was not significantly different from Eq. (2) ($p = 0.07$) and was marginally significantly different from Eq. (1) ($p = 0.05$). Thus, it was concluded that the three pooled equations were functionally comparable at the current level of precision of the measurement and that slice count-based surface area reflected the slice geometric area, and that this algorithm permitted the determination of K.

Application of Correction Algorithms 1 Through 3 to Assessment of Total Left Ventricular Infarct Size

Figure 6 illustrates the relationship between the pathologic infarct size (x-axis) and the tomographic infarct size (y-axis) for the three methods. For all methods, there was a significant linear correlation between the two variables. The parameters of the regression lines for the three methods are summarized in Table 2. For all three methods, the slopes were close to unity (respectively, 0.95, 1.01, and 1.03 for Methods 1 through 3) and the intercepts were close to zero (respectively, −0.3, −0.4, and −0.5). None of the regression lines was different from the line of identity as demonstrated by p values of 0.69, 0.99, and 0.98, respectively, for Methods 1 through 3. The correlation coefficients r were 0.83, 0.84, and 0.85, respectively. The s.e.e.s (%) were 5, 5.1, and 5.1 for the three methods. The relative precisions were very close to each other for the three methods. The relative biases were slightly smaller for Methods 2 and 3 than for Method 1. Thus, the image-based methods provided results that were at least as good as the pathologic-based method (Method 1) results, and all three methods were suited for the determination of infarct size.

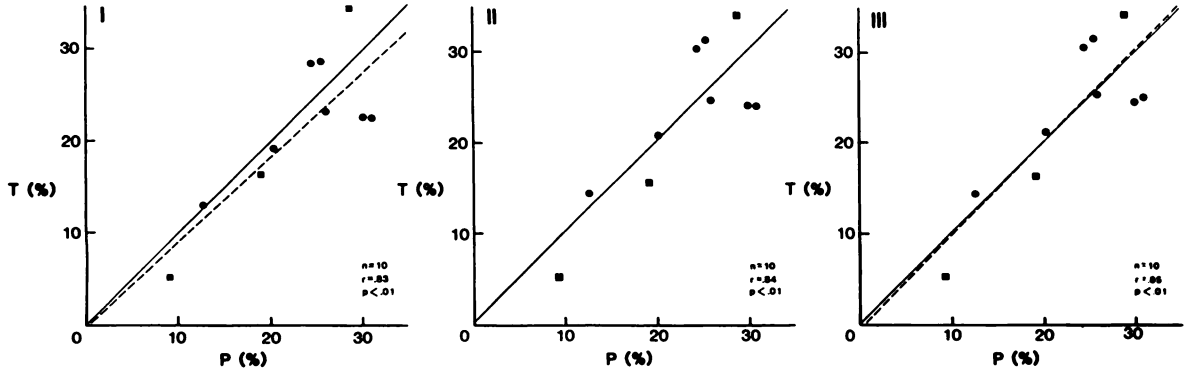

FIGURE 6
Relationship between the tomographic and pathologic infarct size. For all three methods there was a linear relationship between the two variables. None of the regression lines differed from the line of identity.

To determine the effect of the variability of K on total left ventricular infarct size measurement, we compared the infarct size values obtained with K (Algorithm 3), K + 1 s.e.e. and K − 1 s.e.e., using in a dog with LAD infarction in which the pathologic infarct size was 20.2%. The values obtained were, respectively, 21.2% when the correction was done with K, 22.2% when the correction was done with (K + 1 s.e.e.) and 20.6% when the correction was done with (K − 1 s.e.e.). Thus, the variability of K had little effect on left ventricular infarct size measurement.

Dependence of Myocardial Count-Based Slice Area on Slice Distance from the Apex in Humans

A consistent relationship between count-based slice area and fractional slice distance from the apex was observed in humans, with an initial increase of slice area with distance until the mid-ventricular region, and then a decrease at proximity to the base (Fig. 7). A second degree equation ($K = -0.028X^2 + 3.07X + 10.3$; $r^2 = 0.91$, s.e.e. = 6.7%) [Eq. (4)] fit the data best. This equation was significantly different ($p < 0.001$) from Eq. (3) in dogs.

TABLE 2
Parameters of Regression Line for Three Methods for Determining Tomographic Infarct Size Versus TTC

	Method 1	Method 2	Method 3
Intercept	−0.3	−0.4	−0.5
Slope	0.95	1.01	1.03
P_1[†](=)	0.69	0.99	0.98
R[*]	0.83	0.84	0.85
P_2[‡](<)	0.01	0.01	0.01
s.e.e. (%)	5	5.1	5.1
Relative bias (%)	−1.4	−0.2	0.2
Relative precision (%)	4.7	4.7	4.7

[*] R = correlation coefficient.
[†] P_1 = p value for the comparison of the regression line versus the line of identity.
[‡] P_2 = value in testing that the true correlation R is equal to 0.

DISCUSSION

In this study we developed image-based algorithms to determine the contribution of myocardial slice mass to the total left ventricular mass in normal dogs. This was attempted to derive correction factors for determin-

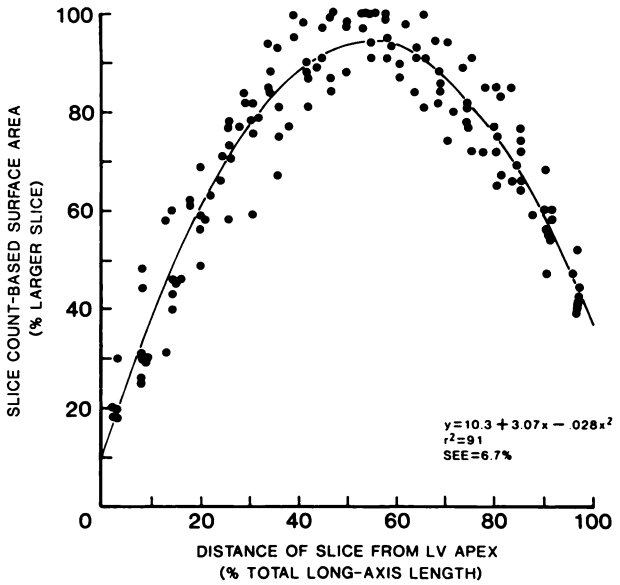

FIGURE 7
Dependence of myocardial slice count-based surface area on slice distance from the apex in eight normal humans.

ing the total left ventricular infarct size from the infarct size of individual tomograms.

Several studies have demonstrated that quantification of experimental infarct size is feasible by ^{201}Tl SPECT. Keyes et al. (*15*) demonstrated that viable and infarcted myocardium could be measured in excised canine hearts by rotational ^{201}Tl SPECT with 360° acquisition and no attenuation or scatter correction. Caldwell et al. (*17*) measured relative myocardial perfusion defect size in dogs using 180° acquisition and no attenuation or scatter correction. In all of these studies, endocardial and epicardial myocardial borders as well as the edge of infarcted area were assigned manually or by a computerized edge detection algorithm.

In a previous study (*21*), we demonstrated that maximum count circumferential profile analysis could be applied to quantify infarct size in individual tomograms, using ^{201}Tl, 180° acquisition and no scatter or attenuation correction. Since with the method of circumferential profile analysis, the infarct size is given as a percentage, it was necessary to develop algorithms accounting for the difference of myocardial slice mass from apex to base. When this correction was not done (uncorrected method) there was as overestimation of LAD infarct size and an underestimation of LCX infarct size. This was due to the fact that this method assumes that all myocardial slices contribute to the same degree to the total left ventricular mass, and overestimates the relative contribution of the apical part of the left ventricle. Thus, infarction involving the apex, such as LAD infarction, will be overestimated. Conversely, infarction involving the mid and basal portions of the left ventricle, such as LCX infarction, will be underestimated.

As expected, correction for slice mass using Algorithm 1 consistently decreased the LAD infarct size by decreasing the relative contribution of the distal slices to the total left ventricular mass and slightly increased the LCX infarct size by increasing the relative contribution of the mid and basal slices to the total left ventricular mass.

Since it may be difficult to gather enough autopsy data from patients with normal hearts, we sought to develop image-based algorithms accounting for the difference of myocardial slice mass from apex to base. Algorithm 2 expressed the geometric surface area of any given slice according to its fractional distance from the left ventricular apex. Since Equations 1 and 2 did not differ significantly, we concluded that these equations were functionally comparable at the level of precision of the measurement and that relative geometric slice area reflected the relative mass of a myocardial slice and that K could be predicted from Algorithm 2. In this method, however, the measurement of slice thickness was dependent on edge detection.

With Algorithm 3, the dependence of count-based slice area on the slice distance from the apex in normal dogs is described. To determine the relative count-based slice area, we used the previous observation of Hoffman et al. (*26*) and Weisenberg et al. (*27*) where, in positron emission tomography, the recovered counts have been demonstrated to depend on wall thickness when the thickness of the object is smaller than 2 FWHM. Their experiments were conducted with three different filters (high, medium, and low resolution) that gave, respectively, FWHM of 11.6, 15.5, and 19.9 mm. Since for object smaller than 2 FMHM there is never a plateau region in the image to allow averaging of several pixel elements, the maximum value was chosen as the best estimate of the concentration of the tracer.

Galt et al. (personal communication), have shown that when imaging spheres of different diameters filled with ^{99m}Tc or a wedge phantom with the same imaging device as the one used in the present study, the recovered counts were also dependent on object size with a near-linear relationship and "that it may be feasible to predict myocardial wall thickness by comparing extracted counts to a standard thickness."

In our study we used a low-resolution filter that gave approximately the same resolution (18 mm FWHM) as the resolution obtained in the PET study. We used the maximum count value as the best representative of the concentration of the tracer and thus of myocardial wall thickness since it was the least attenuated. In our study, the true myocardial wall thickness was not known, nor any conversion factor between counts and thickness. But this was not of importance since we were using count-based slice area normalized to the greatest slice area. Despite the different energy resolution of ^{201}Tl, the dependence of recovered counts on object size was still apparent in our study since Eq. (3) was not significantly different from the Eq. (2) and was only marginally different from Eq. (1). It is possible that use of an attenuation correction would improve the relationship between the three algorithms. We did not use any attenuation correction since no adequate attenuation correction is presently available for ^{201}Tl.

Since for five of six dogs, the equations' % geometric area versus distance and % count-based area versus distance were not different and since the pooled equations were at the most marginally different, we concluded that (a) all three equations were functionally comparable at the level of precision achieved and (b) the relative count-based slice area reflected the relative myocardial slice mass, and (c) K could be predicted from Algorithm 3.

The next step was to develop a comparable equation for human studies. To determine the algorithm we used a similar process as for Method 3 in dogs, since the results obtained using Algorithm 3 were at least as good, as the results obtained using Algorithm 1 and since it is an easy method to use, independent of edge detection.

In humans, a predictable relationship was also observed between % count-based slice area and fractional distance from the apex; as for the experimental data, a second degree equation best fit the data (Fig. 7). This equation was significantly different from Eq. (3), most likely due to differing attenuation factors in the two species, and differing myocardial geometry.

Whether or not this count based area is really representative of the true slice volume in humans remains to be addressed by generating an equation relating true slice mass, measured on autopsied hearts to its fractional distance from the apex. Such comparison will allow to determine if attenuation in humans which is substantially greater than in dogs, would alter slice area estimation from the count-based method, especially in the base of the heart.

APPENDIX

Measurement of slice surface area: If r_1 is the radius of the outer circle and r_2 is the radius of the inner circle, the slice surface area is: $S = \pi(r_1^2 - r_2^2)$. If t is the myocardial wall thickness, and r is the mean radius, r_1 is equal to $(r + t/2)$ and $r_2 = (r - t/2)$.

Thus, $S = \pi(r + t/2)^2 - \pi(r - t/2)^2 = 2\,\pi t \cdot r$, or $S = \pi \cdot d \cdot t$ if d = mean diameter.

NOTE

†(Siemens Rota or Siemens' Orbiter) Searle-Siemens Medical Systems, Inc., Iselin, NJ.

ACKNOWLEDGMENTS

The authors thank Dr. William Ganz for making his animal laboratory available to us and Dr.Yuichi Sato for his help in preparation of the animals. The authors acknowledge Christopher Wong, CNMT, for acquisition of the studies, Rose Goldsmith for assistance in preparation of the figures, and Gregory Kuhl, M.A., for assistance in preparation of the manuscript.

This work was supported in part by NIH SCOR Grant #17651 and grants from the American Heart Association, Greater Los Angeles Affiliate. This study was presented in part at the 32nd Annual Meeting of the Society of Nuclear Medicine, Houston, TX, June 1985.

REFERENCES

1. Page DL, Caulfield JB, Kastor JA, et al. Myocardial changes associated with cardiogenic shock. *N Engl J Med* 1971; 285:133.
2. Sobel BE, Bresnahan GF, Shell WE, et al. Estimation of infarct size in man and its relation to prognosis. *Circulation* 1972; 46:640.
3. Holman BL, Chisholm RJ, Braunwald E. The prognostic implication of acute myocardial infarct scintigraphy with ^{99m}Tc-pyrophosphate. *Circulation* 1978; 57:320.
4. Sobel BE. Infarct size, prognosis, and causal contiguity. *Circulation* 1976; 53:I-146.
5. Holman BL, Goldhaber SZ, Kirsh C-M, et al. Measurement of infarct size using single photon emission computed tomography and technetium-99m pyrophosphate: a description of the method and comparison with patient prognosis. *Am J Cardiol* 1982; 50:503–511.
6. Shell WE, Kjekshus JK, Sobel BE. Quantitative assessment of the extent of myocardial infarction in the conscious dog by means of analysis of serial changes in serum creatine phosphokinase activity. *J Clin Invest* 1973; 52:2579.
7. Norris RM, Whitlock RM, Barratt-Boyes C, et al. Clinical measurement of myocardial infarct size: modification of a method for the estimation of total creatine phosphokinase release after myocardial infarction. *Circulation* 1975; 51:614–620.
8. Roberts AJ, Cipriano PR, Alonso DR, et al. Evaluation of methods for the quantification of experimental myocardial infarction. *Circulation* 1978; 57, 35–41.
9. Poliner LR, Buja LM, Parkey RW, et al. Comparison of different noninvasive methods of infarct sizing during experimental myocardial infarction. *J Nucl Med* 1977; 18:517–523.
10. Botvinick EH, Shames D, Lappin H, et al. Noninvasive quantitation of myocardial infarction with technetium-99m pyrophosphate. *Circulation* 1975; 52:909–915.
11. Nelson AD, Khullar S, Leighton RF, et al. Quantification of thallium-201 scintigrams in acute myocardial infarction. *Am J Cardiol* 1979; 44:664–669.
12. Okada RD, Lim YL, Chesler DA, et al. Quantitation of myocardial infarct size from thallium-201 images: validation of a new approach in an experimental model. *J Am Coll Cardiol* 1983; 3:948–954.
13. Lewis SE, Stokely EM, Devous Sr, et al. Quantitation of experimental canine infarct size with multipinhole and rotating-slanthole tomography. *J Nucl Med* 1981; 22:1000–1005.
14. Keyes JW Jr, Leonard PF, Brody SL, et al. Myocardial infarct quantification in the dog by single photon emission computed tomography. *Circulation* 1978; 58:227–232.
15. Keyes JW Jr, Brady TJ, Leonard PF. Calculation of viable and infarcted myocardial mass from thallium-201 tomograms. *J Nucl Med* 1981; 22:339–343.
16. Tamaki S, Nakajima H, Murakami T, et al. Estimation of infarct size by myocardial emission computed tomography with thallium-201 and its relation to creatine kinase-MB release after myocardial infarction in man. *Circulation* 1982; 66:994–1000.
17. Caldwell JH, Williams DL, Harp GD. Quantitation of size of relative myocardial perfusion defect by single-photon emission computed tomography. *Circulation* 1984; 70:1048–1056.
18. Thompson CJ, Mena I, Maublant JC. Thallium-201 tomographic estimation of left ventricular mass in normal and infarcted canine hearts using a new automated edge-detection program [Abstract]. *J Am Coll Cardiol* 1985; 5:533.
19. Doherty PW, Lipton MJ, Berninger WH, et al. Detection and quantitation of myocardial infarction in vivo using transmission computed tomography. *Circulation* 1981; 63:597–606.
20. Weiss ES, Ahmed SA, Welch MJ, et al. Quantification of infarction in cross sectional canine myocardium in

vivo with positron emission transaxial tomography and ^{11}C-palmitate. *Circulation* 1977; 55:66.
21. Prigent F, Maddahi J, Sato Y, et al. Quantification of myocardial infarct size in the dog using single-photon emission computerized tomography: slice-by-slice comparison of T1-201 tomograms and pathology. *Circulation* 1984; 70:II-450.
22. Fishbein MC, Meerbaum S, Rit J, et al. Early phase acute myocardial infarct size quantification: validation of the triphenyl tetrazolium chloride tissue enzyme staining technique. *Am Heart J* 1981; 101:593.
23. Vivaldi MT, Kloner RA, Schoen FJ. Simulated autopsy detection of early myocardial infarcts: effects of duration of ischemia and autolysis [Abstract]. *J Am Coll Cardiol* 1985; 5:400.
24. Borello JA, Clinthorne NH, Rogers WL, et al. Oblique angle tomography: a restructuring algorithm for transaxial tomographic data. *J Nucl Med* 1981; 22:471.
25. Prigent F, Maddahi J, Sato Y, et al. Single photon emission computerized tomography for quantification of experimental myocardial infarct size. *J Am Coll Cardiol* 1985; 5:440.
26. Hoffman EJ, Huang SC, Phelps ME. Quantitation in positron emission computed tomography: 1. effect of object size. *J Comp Asst Tomogr* 1979; 3:299–308.
27. Weisenberg G, Schelbert HR, Hoffman EJ, et al. In vivo quantification of regional myocardial blood flow by positron emission computerized tomography. *Circulation* 1981; 63:1248–1258.
28. Diamond G, Forrester J. Analysis of probability as an aid in the clinical diagnosis of coronary artery disease. *N Engl J Med* 1979; 300:1350.
29. Maddahi J, Rozanski A, Becerra A, et al. Patients with a calculated very low likelihood of coronary artery disease: an alternative population of cardiac normals [Abstract]. *Circulation* 1982; 66:II-62.
30. BMDP statistical software. Dixon WJ, ed. Los Angeles: University of California Press, 1983.
31. SAS user's guide: statistics, 1982 edition. Cary, NC, SAS Institute, Inc., 1982.
32. Draper N, Smith H. Applied regression analysis, 2nd edition. New York: John Wiley & Sons, 1981.